

0571-7256/15/5804-0453 (C)2015 Springer Science+Business Media New York Original article submitted August 18, 2015. Translated from *Astrofizika*, Vol. 58, No. 4, pp. 487-504 (November 2015).

EXTENDING THE $H\alpha$ SURVEY FOR THE LOCAL VOLUME GALAXIES

I. D. Karachentsev, S. S. Kaisin, and E. I. Kaisina

Special Astrophysical Observatory of the Russian Academy of Sciences; e-mail: ikar@sao.ru

ABSTRACT

Images in the $H\alpha$ emission line are presented for 35 nearby objects observed with the 6-m BTA telescope. Three of them, NGC 3377, NGC 3384, and NGC 3390, are bright E and S0 galaxies, one is an edge-on Sd galaxy UGC 7321, two are remote globular clusters associated with M 31, and the rest are dwarf galaxies of morphological types dIr, dTr, dSph, BCD, and Sm. The measured $H\alpha$ fluxes are used to estimate the integral (SFR) and specific (sSFR) star formation rates for these galaxies. The values of $\log[sSFR]$ for all these objects lie below a limit of $-0.4(\text{Gyr}^{-1})$. We note that the emission disk for the nearest superthin edge-on galaxy UGC 7321 has an extremely large axis ratio of $a/b = 38$.

Keywords: galaxies: star formation

1 Introduction.

Since 2004 a program for surveying nearby galaxies in the Balmer $H\alpha$ line has been under way with the 6-m telescope at the Special Astrophysical Observatory of the Russian Academy of Sciences. The purpose of this program is to determine the star formation rate in the galaxies lying within a fixed local volume by measuring their integral flux in the $H\alpha$ line.

At the beginning of this survey in 2004, the "Catalog of Nearby Galaxies," CNG [1], included 450 galaxies with distances $D < 10$ Mpc. Over the last 10 years, this sample has increased by a factor of two as a result of a wide field survey of the sky in the visible range and in the 21-cm neutral hydrogen line. The latest version of the "Updated Nearby Galaxy Catalog", UNGC [2], contains 869 objects with estimated distances $D < 11$ Mpc and is still being extended in the form of a data base [3] that can be found on the internet at <http://www.sao.ru/lv/lvgdb>.

Thus far we have obtained images in the $H\alpha$ line for ~ 400 nearby galaxies in the northern sky [4-11]. In order to avoid undesirable selection effects we have observed galaxies of all morphological types and luminosities without exception. These $H\alpha$ -images of the galaxies and their $H\alpha$ fluxes, which are given in the data base [3], provide a unique opportunity for research on the distribution of star formation regions in galaxies of different types with high spatial resolution. We have published a survey of the basic characteristics of star formation in nearby galaxies [12] with data on measurements of the $H\alpha$ fluxes for ~ 200 galaxies in the Local volume taken into account by a program analogous to that initiated by Kennicutt [13].

Detailed charts of the distribution of ionized hydrogen in nearby galaxies together with data on the distribution of young blue stars in these galaxies obtained by the GALEX survey [14] make it possible to establish the star formation rate on time scales ranging from ~ 10 to ~ 100 million years. Multiaperture observations of these galaxies in the HI line [15,16] can be used to study the distribution and kinematics of neutral hydrogen and, thereby, to gain a better understanding of the mechanism for conversion of the gas into stars. The massive $H\alpha$ -survey of nearby galaxies also serves as a basis for selection and subsequent analysis of the kinematics of the most active objects with the aid of a Fabry-Perot etalon [17,18].

Here we present $H\alpha$ -images, values of the $H\alpha$ -flux, and estimates of the star formation rate (SFR) for 35 objects in the Local volume. Of these objects, 30 are dwarf galaxies, 3 are massive E, S0 galaxies, and 2 are globular clusters in the remote periphery of M 31.

2 Observations and data processing.

The galaxies were observed in the primary focus of the BTA telescope with the SCORPIO focal reducer equipped with a 2048×2048 pixel CCD array over the period from October 2014 through March 2015. The optical system provided a field of view of $\sim 6'$ with a scale of $0.185''/\text{pixel}$. An interference $H\alpha$ filter with a width $\text{FWHM}=75\text{\AA}$ and an effective wavelength of 6555\AA was used for the observations. Images in the continuum were taken with middle-band centered SED607 ($\Delta\lambda = 167\text{\AA}$, $\lambda_e = 6063\text{\AA}$) and SED707 ($\Delta\lambda = 207\text{\AA}$, $\lambda_e = 7036\text{\AA}$) filters. All the objects were observed with the same set of filters, since the galaxies had a small range of radial velocities. The total exposure was about 20 min for each object.

The observational data were processed by a set of standard procedures that included dark frame subtraction, then the image was normalized to a flat field obtained at twilight and traces of cosmic particles were eliminated by comparing images and sky background subtracted. The continuum images were normalized to the image in the $H\alpha$ -filter using 10–30 stars and then subtracting. The $H\alpha$ -flux of a galaxy was determined from the $H\alpha$ -image after background subtraction. The flux was calibrated using images of spectrophotometric standard stars observed on the same nights. The typical error in the measurement of the logarithm of the $H\alpha$ -flux was determined mainly by the weather conditions and was ~ 0.1 dex.

3 Observational results.

A mosaic of 35 pairs of observed images of galaxies is shown in Fig. 1. The left images of each pair correspond to combined exposure in the $H\alpha$ and the continuum, and the right images, to the image in $H\alpha$ with the continuum subtracted. The name of each object, the image scale, and the "north and east" orientations are indicated on the right images. Bright stars, as well as stars and galaxies with an anomalous color, show up in the right images as residual "stump". Another reason for imperfection of the subtracted images was variable atmospheric turbulence. A faint interference pattern can be seen in some of the images owing to deficiencies in the procedure for flat field division.

We corrected the measured ranges (in units of $\text{erg}/\text{cm}^2/\text{s}$) of the $H\alpha$ -fluxes, $F(H\alpha)$, of the galaxies for Galactic absorption in accordance with [19]. The corrected value $F_c(H\alpha)$ served as an estimate of the integral star formation rate of a galaxy [20] (in units of M_\odot/year):

$$\log[SFR] = \log F_c(H\alpha) + 2 \log D + 8.98, \quad (1)$$

where D is the distance to a galaxy in Mpc. Here we neglect the contribution to the flux from the $[NII]$ emission doublet, as well from internal absorption in the galaxy, since both effects are small for dwarf galaxies [21,13], which are a majority of the observed objects. The only exception was the spiral galaxy UGC 7321, which is seen edge on and has an internal absorption of 0.66^m in the $H\alpha$ -line [21].

The main parameters of the observed galaxies are summarized in Table 1, the columns of which list the following: (1) the name of the galaxy; (2) the equatorial coordinates at epoch 2000.0; (3) the integral B -magnitude; (4) the morphological type according to data from the UNGC catalog [2]; (5) the distance in Mpc [2]; (6) the method by which this distance was determined (*rgb* from the luminosity of stars in the red giant branch; *sbf* from surface brightness fluctuations; *TF* from the Tully-Fisher relation between the rotation amplitude of a galaxy and its luminosity; *mem* from membership in known groups; *h* from the radial velocity relative to the centroid of the Local group for a Hubble parameter $H_0 = 73$ km/s/Mpc; and, *txt* from the texture of the image of a dwarf galaxy (this estimate is extremely uncertain)); (7) the logarithm of the $H\alpha$ -flux we have measured; (8) the logarithm of the integral star formation rate according to the formula given above; (9) the integral star formation rate of the galaxy,

$$\log[SFR(FUV)] = \log F_c(FUV) + 2 \log D - 6.78, \quad (2)$$

determined from its far ultraviolet flux ($\lambda_e = 1539\text{\AA}$, FWHM = 269\AA) measured by the GALEX satellite [14] with a correction for absorption of light in our Galaxy; and, (10) the specific star formation rate normalized to unit stellar mass of the galaxy. Several estimates of the $H\alpha$ -flux obtained through cirrus are indicated by a colon.

4 Distinctive features of the observed objects.

PAndAS-04, PAndAS-56. Two globular clusters at the distant periphery of M 31 from the catalog of [22] with projected distances from the center of M 31 of 124 and 103 kpc, respectively. Such isolated objects may be centers to which intergalactic gas accretes. Data from GALEX [14] show that PAndAS-04 has a significant flux in the far ultraviolet. But, according to our measurements, the $H\alpha$ -flux from both globular clusters lies below the detection threshold.

[TT2009]25, [TT2009]30. Two candidates for satellites of the massive spiral galaxy NGC 891 detected in [23]. A recent measurement of the radial velocity of the brighter dwarf object [TT2009]25 confirms its physical coupling to the galaxy NGC 891 [24]. Both dwarf galaxies have been detected as faint FUV sources in the GALEX survey, but their $H\alpha$ -fluxes were below the detection threshold in our observations.

KKH30, NGC2146sat. Two isolated dwarf galaxies with low surface brightnesses and unknown radial velocities. There are no structural details of them, but both galaxies have fully symmetric shapes. $H\alpha$ -fluxes have not been detected from them, but according to the GALEX survey, both are faint FUV sources. Based on the combination of these characteristics, they have been classified as dTr type dwarf galaxies, intermediate between dIr and dSph. The distances to the two galaxies are extremely uncertain. It is possible that these dwarf

Таблица 1: Main Properties of the Observed Galaxies.

Name	RA (2000.0) Dec	B_t	T	D	method	log F(H α)	log SFR (H α)	log SFR (FUV)	log sSFR (H α)
(1)	(2)	mag	(4)	Mpc	(6)	erg/cm ² s	M_{\odot} /yr	M_{\odot} /yr	yr ⁻¹
(1)	(2)	(3)	(4)	(5)	(6)	(7)	(8)	(9)	(10)
PAndAS-04	000442.9+472142	18.4	g.c	0.78	mem	< -15.71	< -6.82	-5.67	< -12.42
PAndAS-56	012303.5+415511	17.6	g.c	0.78	mem	< -14.53	< -5.72	< -6.47	< -11.50
[TT2009]25	022112.4+422151	17.9	dTr	9.8	mem	< -15.41	< -4.39	-4.16	< -11.58
[TT2009]30	022254.7+424245	18.9	dIr	9.8	mem	< -15.29	< -4.27	-4.25	< -11.07
KKH 30	051742.0+813727	17.5	dTr	9.0	txt	< -15.12	< -4.17	-3.53	< -11.46
N2146sat	062413.2+775753	17.5	dTr	9.0	txt	< -15.11	< -4.16	-3.82	< -11.45
AGC188955	082137.0+041901	17.5	dIr	14.5	TF	-13.43	-2.11	-2.24	-9.73
LV0853+3318	085326.8+331819	19.5	dIr	9.4	mem	-14.15	-3.20	-3.60	-9.66
LV0926+3343	092609.4+334304	17.8	Sm	10.3	TFb	-13.76	-2.74	-2.39	-10.04
LV1017+2922	101726.5+292211	16.6	BCD	5.4	h	-13.97	-3.50	-	-10.64
AGC749315	102906.4+265438	19.1	BCD	11.0	h'	-15.00	-3.91	-3.04	-10.66
AGC200499	103808.0+102251	14.4	BCD	13.9	h	-13.05	-1.73	-	-10.72
NGC3377	104742.4+135908	11.2	E	10.9	sbf	-12.84	-1.75	-2.25	-12.18
NGC3384	104816.9+123745	10.9	S0	11.4	sbf	< -15.32	< -4.20	-	< -14.94
NGC3413	105120.7+324558	13.2	Sm	12.0	TF	-12.13	-0.92	-1.04	-10.27
KKH 73	115006.4+554700	17.3	dTr	9.0	txt	< -15.12	< -4.23	< -4.48	< -11.49
NGC3990	115735.6+552731	13.4	S0	10.3	sbf	< -15.12	< -4.10	-	< -13.63
LV1157+5638	115754.2+563816	17.1	dIr	7.0	h	-13.0:	-2.3:	-2.86	-9.5:
UGC7257	121503.0+355731	14.4	Sm	8.8	TF	-12.22	-1.32	-1.31	-9.63
UGC7321	121734.0+223225	14.1	Sd	17.2	TF	-12.71	-0.97	-0.23	-10.54
LV1218+4655	121811.1+465501	16.8	Sm	6.5	h	-14.2:	-3.6:	-2.89	-10.8:
LV1219+4718	121927.2+471845	18.0	dIr	7.8	mem	< -15.19	< -4.41	-3.81	< -11.28
KK136	122040.6+470003	17.5	dSp	h 7.8	mem	< -15.08	< -4.30	-	< -12.08
KUG1218+387	122054.9+382549	15.4	BCD	8.0	h	-13.52	-2.71	-2.12	-10.65
UGC7427	122155.0+350305	15.9	dIr	9.7	TF	-13.13	-2.17	-	-10.06
DDO123	122608.1+581921	14.5	Sm	10.5	TF	-12.8:	-1.8:	-	-10.4:
SBS1224+533	122652.6+530619	16.1	BCD	5.4	h	-13.4:	-3.0:	-2.65	-10.3:
DDO131	123158.6+294235	15.3	dIr	8.1	mem	-12.91	-2.09	-1.94	-10.09
NGC4509	123306.8+320530	14.1	BCD	10.1	TF	-12.20	-1.20	-1.26	-9.94
IC3583	123643.5+131534	13.3	Im	9.5	rgb	-12.62	-1.63	-1.24	-10.44
UGCA294	124438.1+282821	14.8	BCD	9.9	TF	-12.7:	-1.7:	-1.57	-10.1:
IC3840	125146.1+214407	16.9	dIr	5.5	TF	-13.60	-3.10	-2.69	-10.15
DDO169NW	131520.1+473237	18.0	dIr	4.2	mem	-13.84	-3.60	-3.02	-9.92
CGCG189-050	131704.9+375708	15.6	BCD	5.0	h	-12.78	-2.39	-	-9.84
AF7448-001	225935.3+164611	17.2	dIr	5.0	TF	-13.63	-3.16	-3.24	-10.11

systems are peripheral satellites of the peculiar galaxy NGC 2146, the distance to which is estimated to be 18 Mpc [25].

AGC188955, AGC749315, AGC200499. Dwarf galaxies of later types observed in the "blind" ALFALFA *HI*-survey [26]. Compact star formation regions can be seen in each of these three objects.

LV0853+3318, LV0926+3343. Two emission dwarf galaxies in the region of the nearby Gemini-Leo cosmic void. The first is a satellite of the massive spiral NGC 2683, the distance to which is ascribed [27] to its dwarf companion.

NGC 3377, NGC 3384. These type E and S0 galaxies belong to the brightest members of the Leo I group. The distances to them have been measured using surface brightness fluctuations [28]. The central part of NGC 3377 manifests emission in the $H\alpha$ -line, as well as in the far ultraviolet.

NGC 3413. A peculiar compact galaxy of a later type with an emission ring seen nearly from the edge-on and a bright central emission region.

UGC 7257. An isolated Sm galaxy with radial velocity $V_{LG} = 957$ km/s at a distance of 8.8 Mpc. This galaxy is distinguished by an abundance of star formation regions that form a spiral-shaped structure with a bright *HII*-complex at its northern edge.

UGC 7321. This Sd galaxy seen strictly edge-on, has radial velocity $V_{LG} = 339$ km/s, and is at a distance of 17.2 Mpc [2]. It belongs to the unusual Coma I group of galaxies which has a peculiar velocity of about -700 km/s [29]. The emission disk of this galaxy, outlined by *HII*-regions, has a record high axis ratio of $a/b = 38$. NGC 7321 is the closest and most distinct example of a "superthin" disk galaxy.

LV1219+4718, KK 136. Both galaxies are indicated in the data base [3] as presumed satellites of the massive spiral NGC 4258, the periphery of which is visible in the lower right corner of the image of LV1219+4718. The radial velocities of these galaxies have not yet been measured. The regular shape of the dSph structure of the galaxy KK 136 and its lack of $H\alpha$ and FUV emission may be indirect evidence of gas being swept out from KK 136 as it interacts with NGC 4258. In the case of the dIr galaxy LV1219+4718, the absence of $H\alpha$ -emission plus a substantial FUV flux probably indicates that this is a distant background galaxy with a substantial radial velocity that shifts the $H\alpha$ -line beyond the limits of the filter that was used.

UGC 7427. This irregular dwarf system has a dumbbell shape with two ring-like emission regions. It may be the result of the merger of two dwarf galaxies with roughly equal masses.

DDO 123 = UGC 7534. This is an Sm type galaxy with a bright star projected onto its southern side. The body of the galaxy contains many small compact *HII* regions. The horizontal line in the image is caused by the passage of a satellite during the exposure time.

SBS1224+533 = MCG+09-20-182. A blue compact galaxy from the Second Byurakan Survey [30] with a radial velocity of $V_{LG} = 390$ km/s.

DDO 131. This is an irregular galaxy with a low surface brightness. It is probably a satellite of the spiral galaxy NGC 4559, to which the distance is 8.1 Mpc. Besides compact *HII* regions, it has 4 emission rings with angular diameters of $5-10''$ which may be residues of supernova outbursts.

NGC 4509 = Mrk 773. A compact dwarf galaxy with a high surface brightness and a loop of small emission knots on its northern side.

IC 3583 = VCC 1686. An Sm type galaxy with a radial velocity of $V_{LG} = 1024$ km/s. In the sky it lies near the center of the cluster of galaxies in Virgo. Given its distance, $D = 9.5$ Mpc measured by the Hubble

Space Telescope [31], IC 3583 is not a member of a cluster but lies in front of a cluster at a distance of ~ 7 Mpc from its center. In the continuum image, the galaxy has an asymmetric shell that gives no indication of $H\alpha$ emission.

UGCA 294 = Haro33. A blue compact dwarf galaxy with emission knots that are almost in contact with one another.

IC 3840. An irregular dwarf galaxy of low surface brightness. There is a narrow emission arc or a fragment of an annular structure on its northern side.

DDO 169NW. A diffuse “granular” satellite of the galaxy DDO 169 = UGC 8331 lying $3'$ to the north west of its center. The ratio of the hydrogen mass to the luminosity of DDO 169NW is high [32]. The major $H\alpha$ -flux of DDO 169NW fits within a faint diffuse component distributed over the entire body of the satellite.

CGCG 189-050. This is a compact blue galaxy with radial velocity $V_{LG} = 368$ km/s. It is probably a distant satellite of the massive spiral galaxy NGC 4736.

AF 7448-001. An irregular dwarf galaxy discovered in the AGES HI -survey [33]. The major $H\alpha$ -flux from it is concentrated in a single compact HII region.

5 Concluding comments.

The data in the Table 1 show that the star formation rate has been estimated by two independent methods for more than 3/4 of the observed galaxies: based on the flux in the $H\alpha$ -line and based on the far ultraviolet flux FUV . The average difference in the star formation rates according to these two methods is $\langle \log SFR(H\alpha) - \log SFR(FUV) \rangle = -0.18 \pm 0.10$ with a mean square deviation of 0.40. It has shown repeatedly [34, 12, 13] that determinations of the star formation rate based on the $H\alpha$ -flux for dwarf galaxies yield a systematic underestimate of the SFR compared to measurements based on the FUV flux. This difference is larger when the luminosity of the dwarf galaxy is lower and its surface brightness is lower. It has been noted [34] that the initial stellar mass function can be substantially different for dwarf and spiral galaxies at its bright end. Because of this, the empirical normalization $SFR(H\alpha) = SFR(FUV)$ for massive disks is not entirely suitable for dwarf systems. Individual differences in the estimates of $SFR(H\alpha)$ and $SFR(FUV)$ can also be caused by the variability in the star formation rate that is typical of dwarf galaxies. The $SFR(FUV)$ estimates typically apply to a time interval of ~ 100 Myr, while the values of $SFR(H\alpha)$ correspond to an interval of $\Delta t \sim 10$ Myr. At the time of the maximum of a star formation burst, $SFR(H\alpha)/SFR(FUV)$ can be substantially greater than unity for irregular and blue compact galaxies.

According to observational data [12,35,36], the specific star formation rate $sSFR = SFR/M^*$ relative to unit stellar mass of the galaxy does not exceed an upper bound of $(SFR)_{max} \simeq -9.4 \cdot \text{dex} (\text{yr}^{-1})$. This empirical condition is satisfied for 99% of galaxies of all morphological types and is an important characteristic of the process by which gas is transformed into stars in the current epoch. As the data in the last columns of the table show, this limit is obeyed by the estimates of $SFR(H\alpha)$ and $SFR(FUV)$ for all the galaxies we have observed. We emphasize that the existence of an empirical upper bound $(SFR)_{max}$ for galaxies has not yet received a clear theoretical explanation.

Acknowledgements. This work was supported by grants No. 15–52–45004 and 13–02–00780 of the Russian Foundation for Basic Research (RFFI) and the new observational data for completing the data base at

http://www.sao.ru/lv/lvgdb were obtained with the support of a grant from the Russian Science Foundation (project No. 14-12-00965).

REFERENCES.

1. *I.D.Karachentsev, V.E.Karachentseva, W.K.Huchtmeier, and D.I.Makarov*, *Astron. J.*, **127**, 2031, 2004 =CNG
2. *I.D.Karachentsev, D.I.Makarov, and E.I.Kaisina*, *Astron. J.*, **145**, 101, 2013 =UNGC
3. *E.I.Kaisina, D.I.Makarov, I.D.Karachentsev, and S.S.Kaisin*, *Astrophys. Bull.*, **67**, 115, 2012
4. *S.S.Kaisin, and I.D.Karachentsev*, *Astrophysics*, **49**, 287, 2006
5. *I.D.Karachentsev, and S.S.Kaisin*, *Astron. J.*, **133**, 1883, 2007
6. *S.S.Kaisin, and I.D.Karachentsev*, *Astron. and Astrophys.*, **479**, 60, 2008
7. *I.D.Karachentsev, and S.S.Kaisin*, *Astron. J.*, **140**, 1241, 2010
8. *S.S.Kaisin, I.D.Karachentsev, and E.I.Kaisina*, *Astrophysics*, **54**, 315, 2011
9. *S.S.Kaisin, and I.D.Karachentsev*, *Astrophysics*, **56**, 305, 2013
10. *S.S.Kaisin, and I.D.Karachentsev*, *Astrophys. Bull.*, **68**, 381, 2013
11. *S.S.Kaisin, and I.D.Karachentsev*, *Astrophys. Bull.*, **69**, 390, 2014
12. *I.D.Karachentsev, and E.I.Kaisina*, *Astron.J.*, **146**, 46, 2013
13. *J.C. Lee, R. C. Kennicutt, J. G. Funes, et al.*, *Astrophys. J.*, **692**, 1305, 2009
14. *A.Gil de Paz, S.Boissier, B.F.Madore et al.*, *Astrophys.J.Suppl.*, **173**, 185, 2007
15. *A.Begum, J.N.Chengalur, I.D.Karachentsev, M.E. Sharina, and S.S.Kaisin*, *MNRAS*, **386**, 1667, 2008
16. *S.Roychowdhury, J.N. Chengalur, A. Begum, and I.D. Karachentsev*, *MNRAS*, **404L**, 60, 2010
17. *A.V. Moiseev*, *Astrophys. Bull.*, **69**, 1, 2014
18. *A.V. Moiseev, A.V. Tikhonov, and A. Klypin*, *MNRAS*, **449**, 3568, 2015
19. *D.J. Schlegel, D.P. Finkbeiner, and M.Davis*, *Astrophys. J.*, **500**, 525, 1998
20. *R.C. Kennicutt*, *Annu. Rev. Astronom. Astrophys.* **36**, 189, 1998
21. *M.A.W. Verheijen*, *Astrophys. J.*, **563**, 694, 2001
22. *A.P. Huxor, A.D.Mackey, A.M.N.Ferguson, et al.*, *MNRAS*, **442**, 2165, 2014
23. *N. Trentham, and R.B. Bully*, *MNRAS*, **398**, 722, 2009
24. *I.D. Karachentsev, M.E. Sharina, D.I. Makarov, et al.*, *Astrophysics*, **58**, 331, 2015
25. *A. Adamo, L.J. Smith, J.S. Gallagher, et al.*, *MNRAS*, **426**, 1185, 2012
26. *M.P. Haynes, R. Giovanelli, A.M. Martin, et al.*, *Astron. J.*, **142**, 170, 2011
27. *I.D. Karachentsev, R.B. Tully, L.N.Makarova, et al.*, *Astrophys. J.*, **805**, 144, 2015
28. *L.Ferrarese, J.R.Mould, R.C.Kennicutt, et al.*, *Astrophys. J.*, **529**, 745, 2000
29. *I.D. Karachentsev, O.G. Nasonova, and H.M. Courtois*, *Astrophys. J.*, **743**, 123, 2011
30. *B.E. Markarian*, *Astrofizics*, **12**, 389, 1976
31. *I.D. Karachentsev, R.B. Tully, Po-Feng Wu, E.J. Shaya, and A.E. Dolphin*, *Astrophys. J.*, **782**, 4, 2014
32. *R.A. Swaters*, PhD Thesis, Groningen, 1999
33. *R.Taylor, R.F.Minchin, H.Herbst, and R.Smith*, *MNRAS*, **442L**, 46, 2014
34. *J.Pflam-Altenburg, C.Weidner, and P.Kroupa*, *Astrophys. J.*, **671**, 1550, 2007
35. *I.D.Karachentsev, V.E.Karachentseva, O.V.Melnyk, and H.M.Courtois*, *Astrophys. Bull.*, **68**, 243, 2013

36. *V.E.Karachentseva, O.V.Melnyk, and I.D.Karachentsev*, *Astrofizics*, **57**, 5, 2014

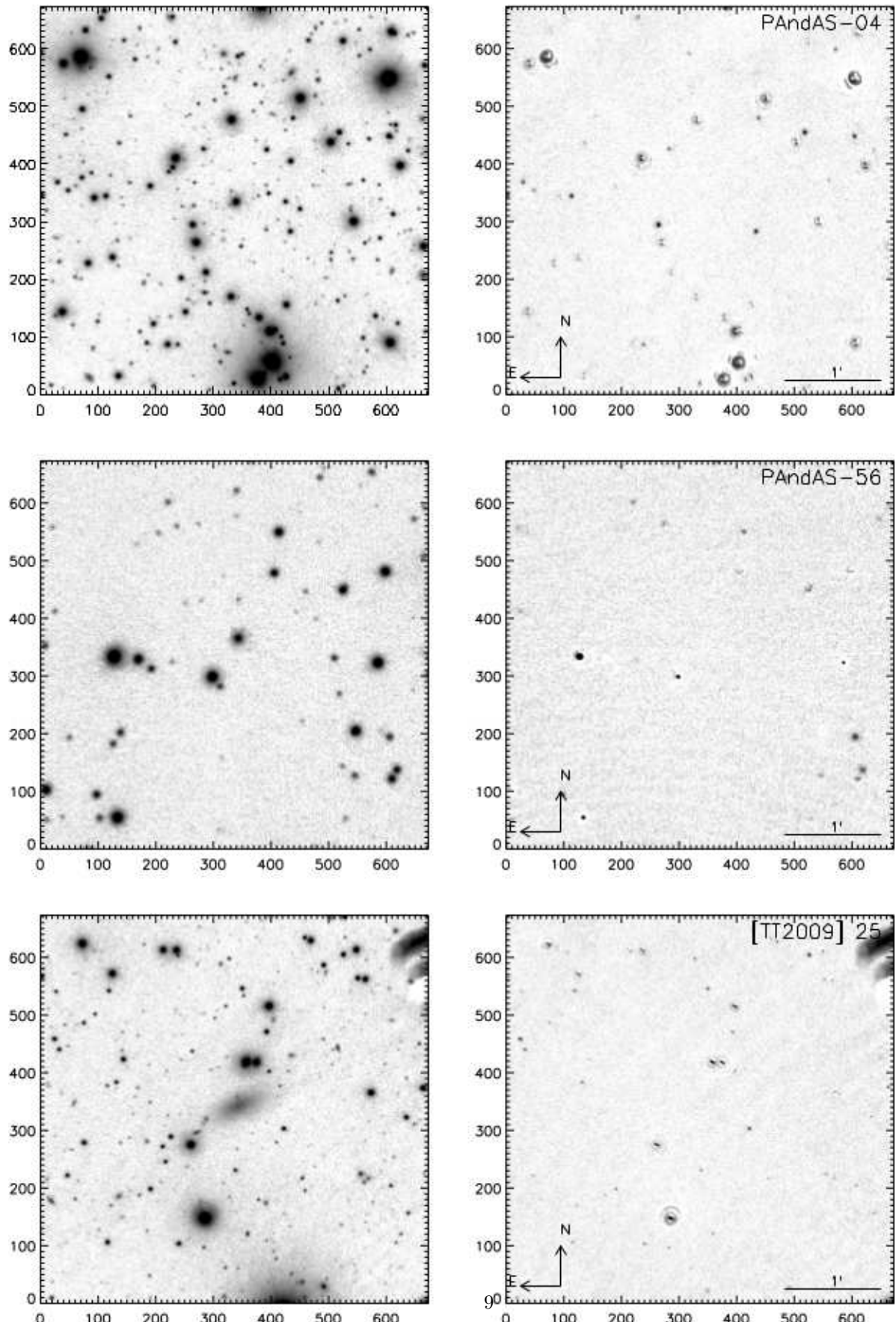


FIG. 1: A mosaic of images of objects in the Local volume. The images on the left of each pair are the sum of exposures in the $H\alpha$ line and the continuum, and the images on the right correspond to the “ $H\alpha$ -continuum” difference. The angular scale and orientation are indicated in the bottom corners of the images on the right.

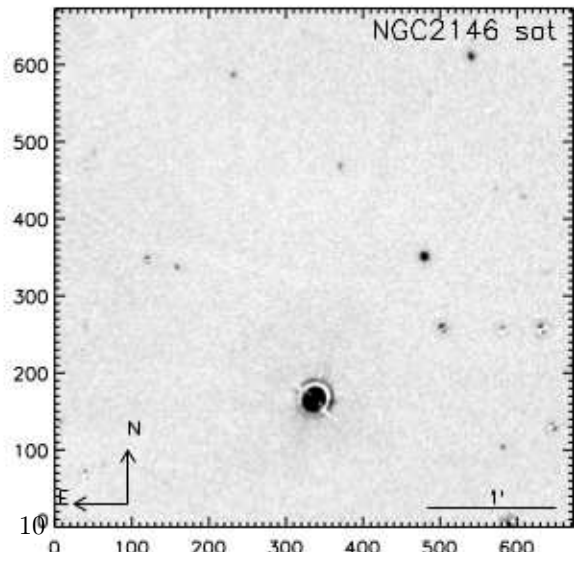
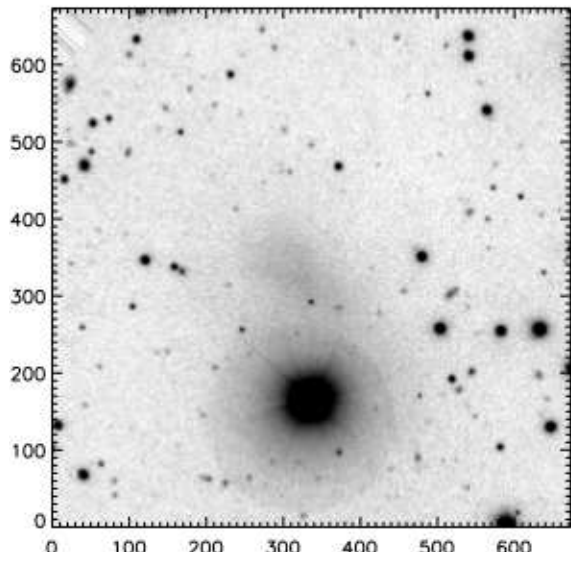
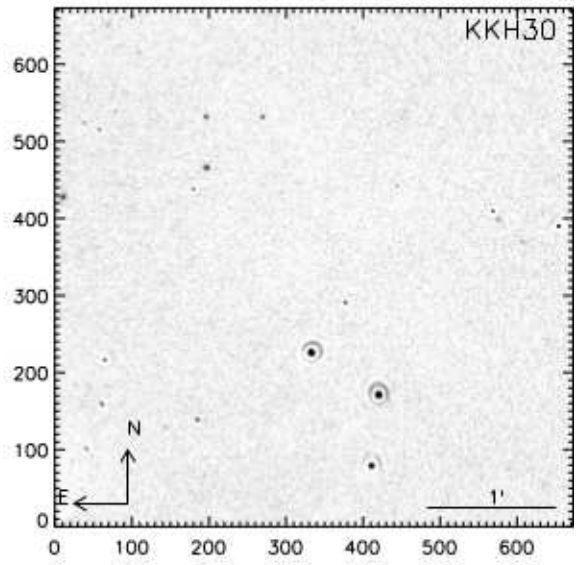
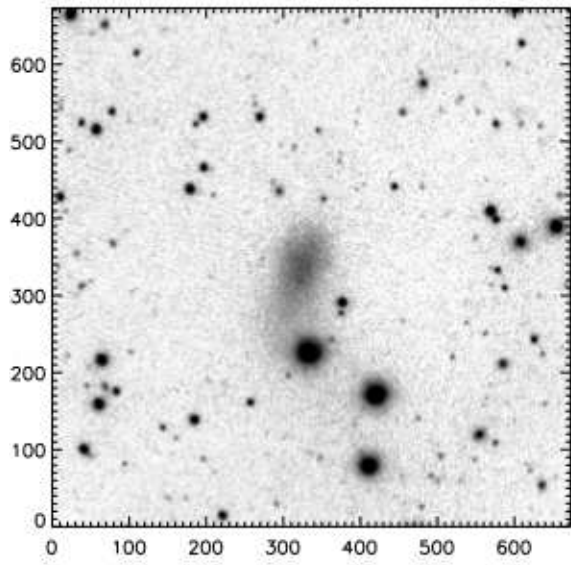
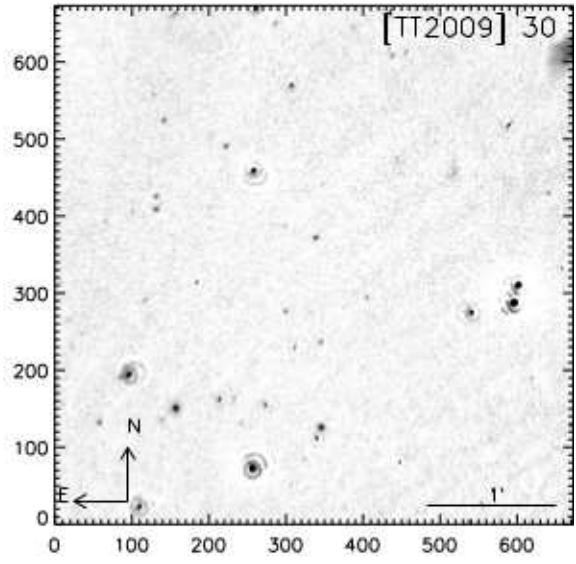
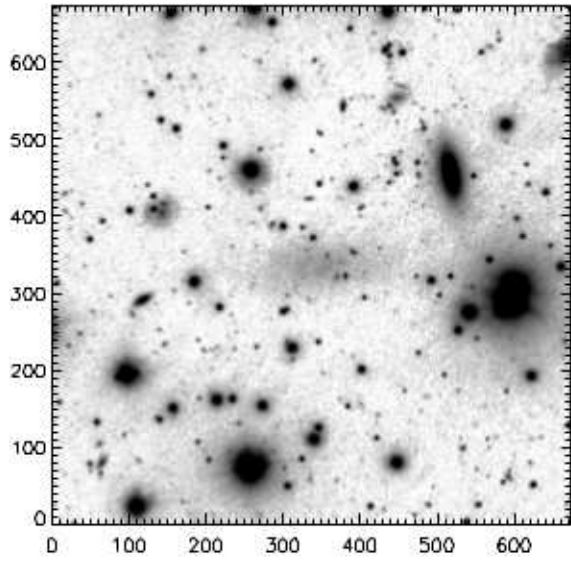


FIG. 1: Continued.

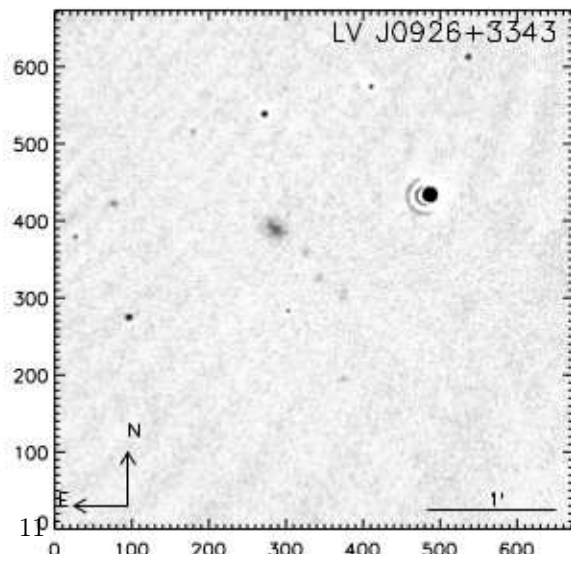
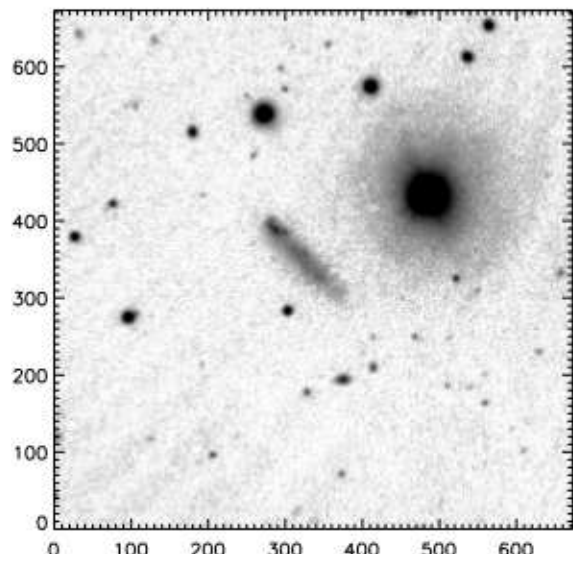
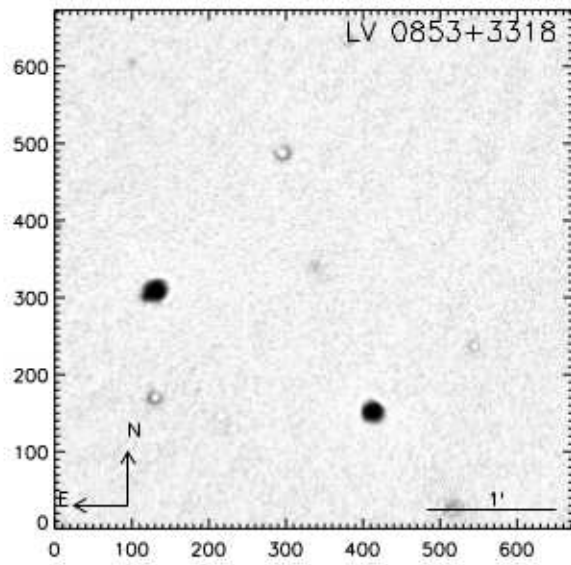
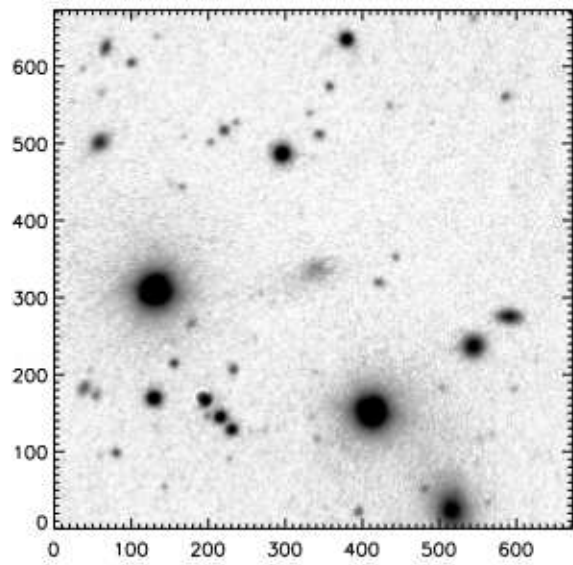
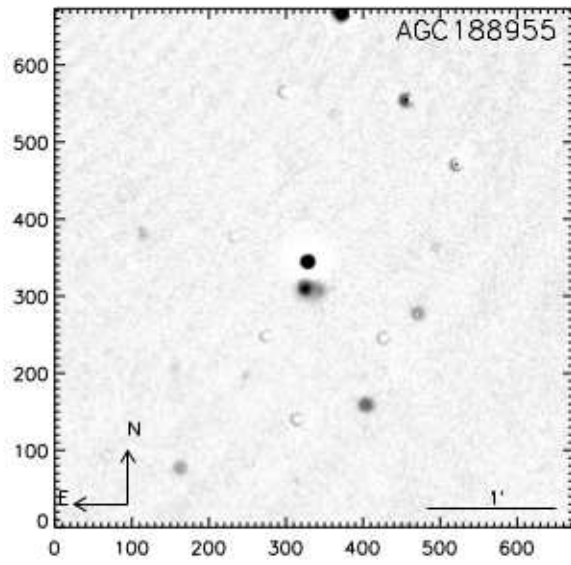
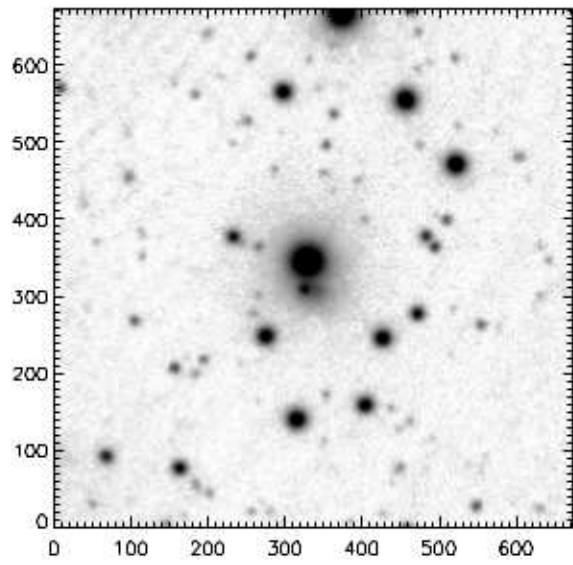


FIG. 1: Continued.

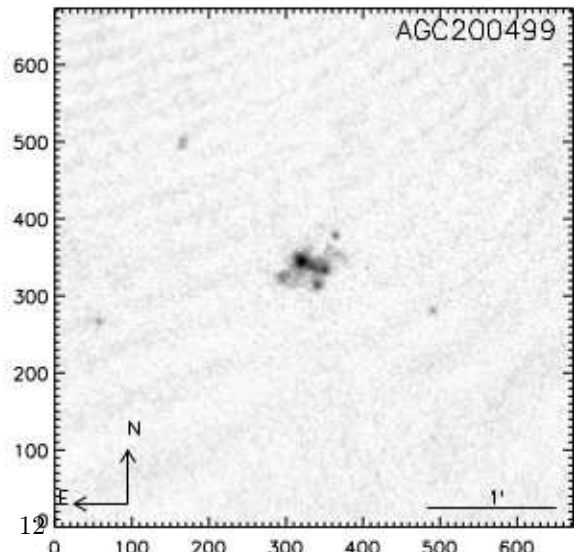
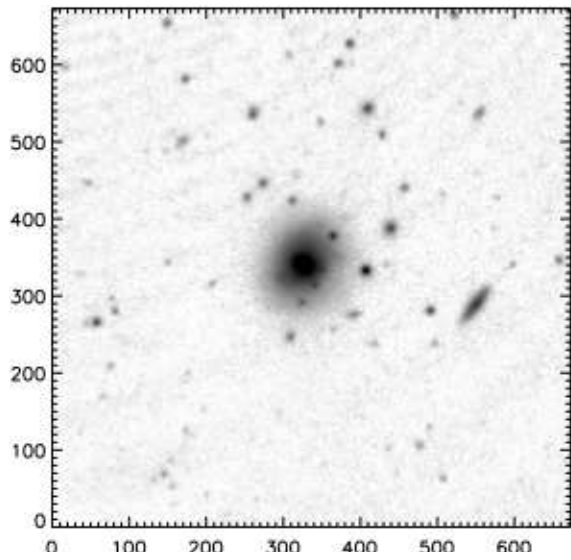
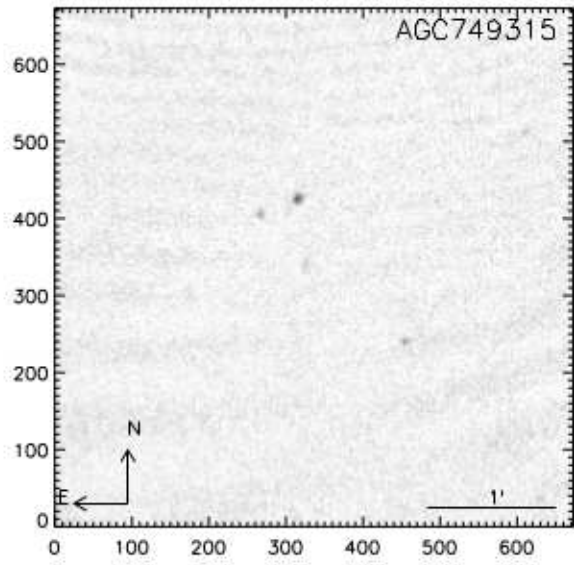
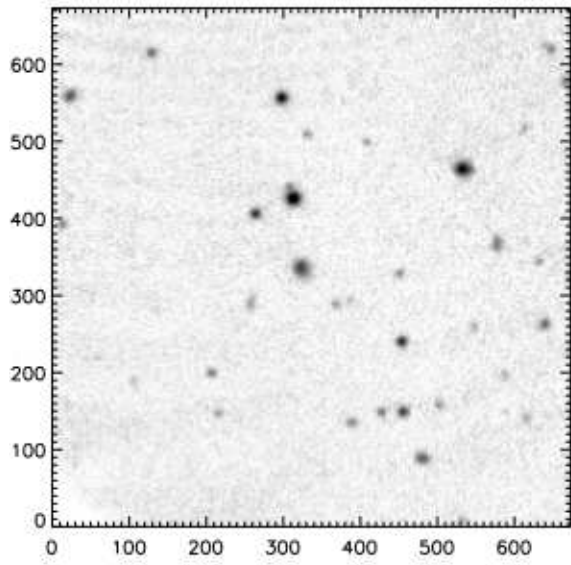
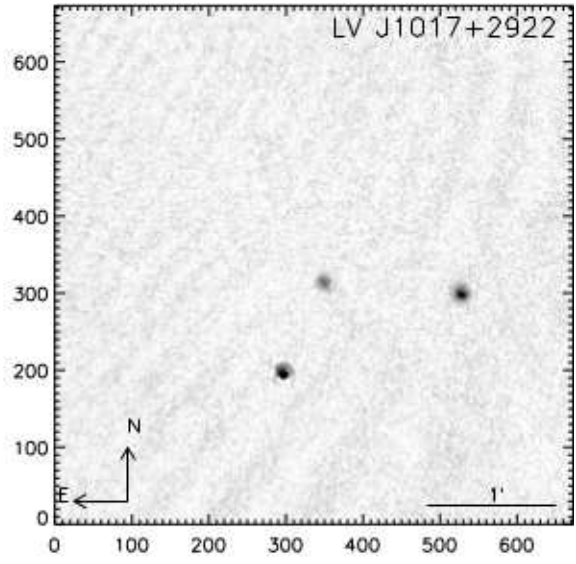
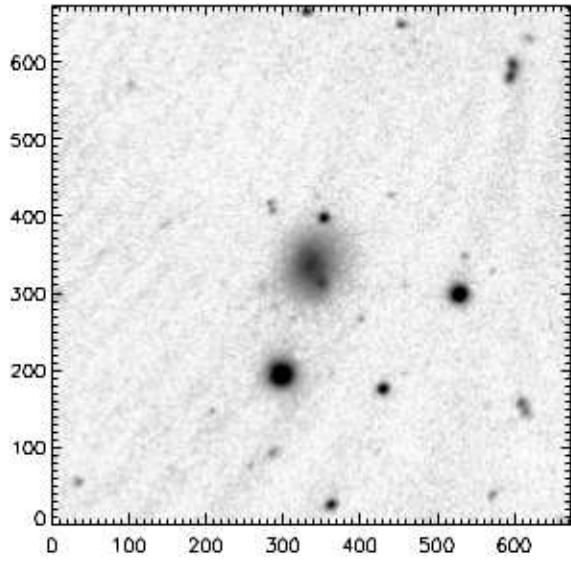


FIG. 1: Continued.

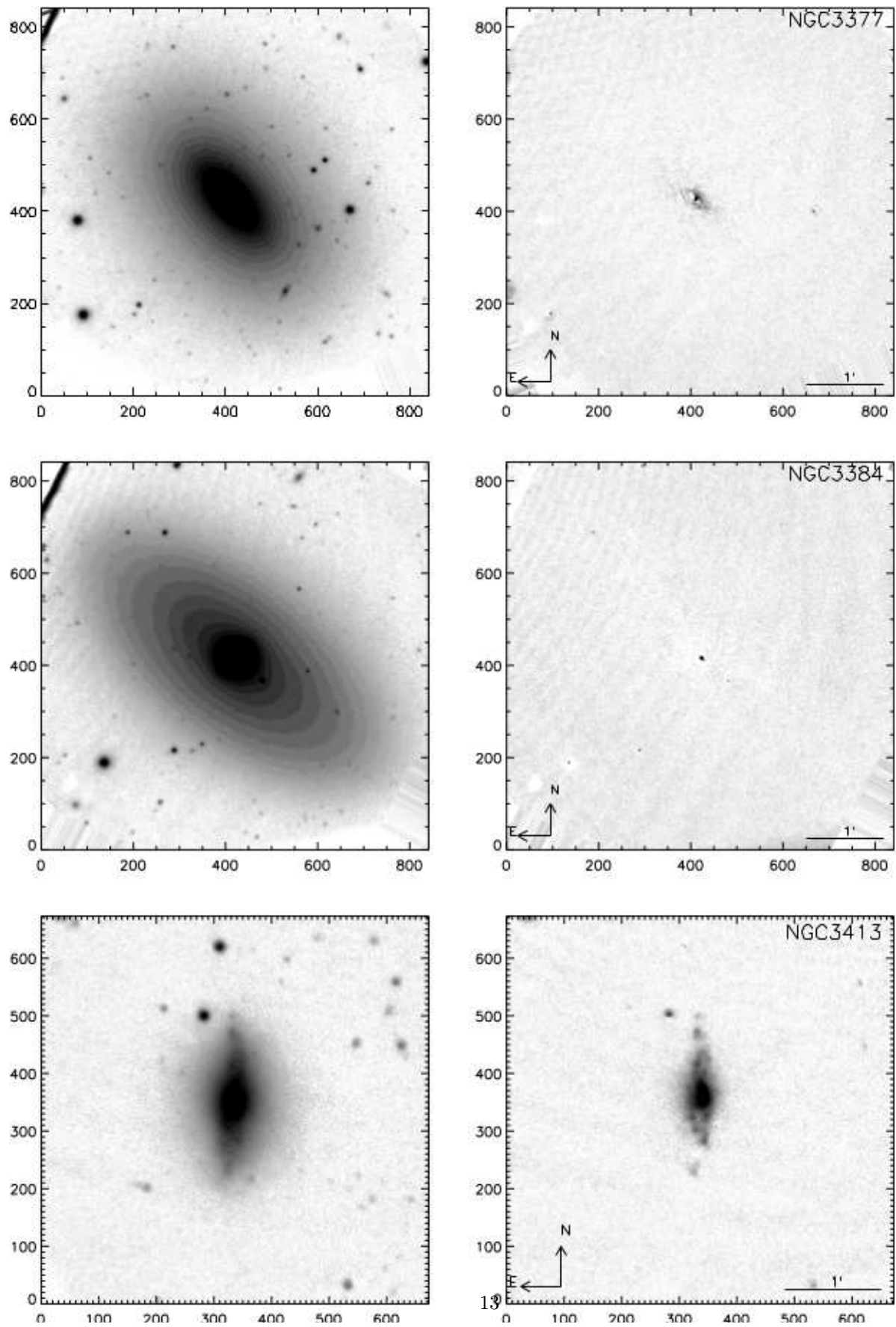


FIG. 1: Continued.

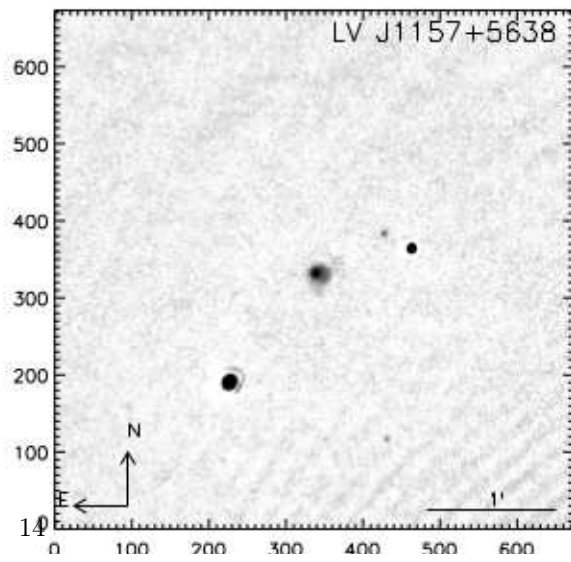
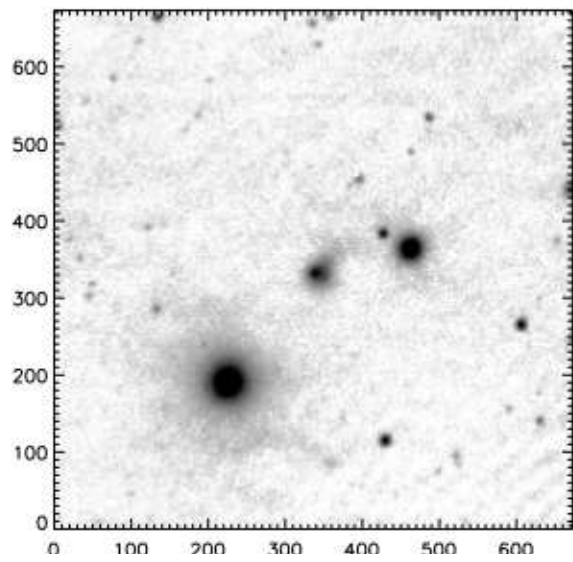
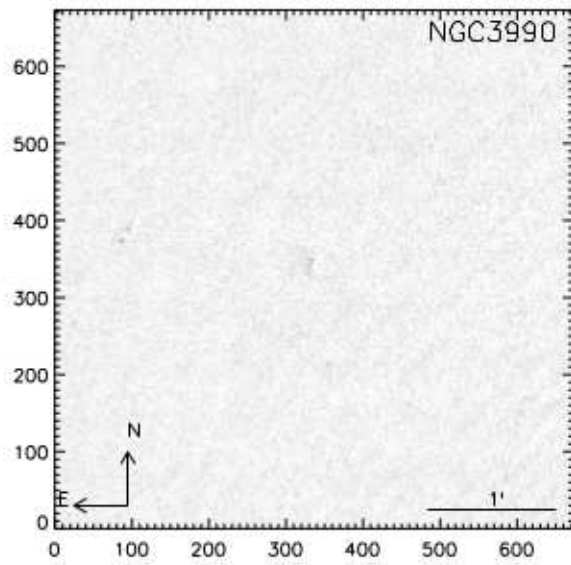
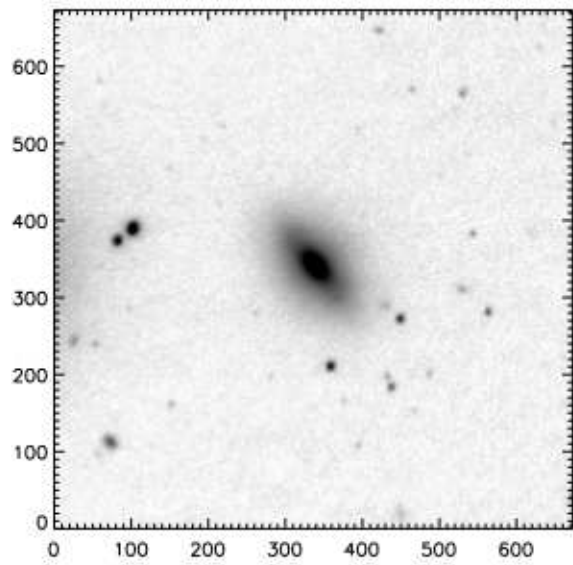
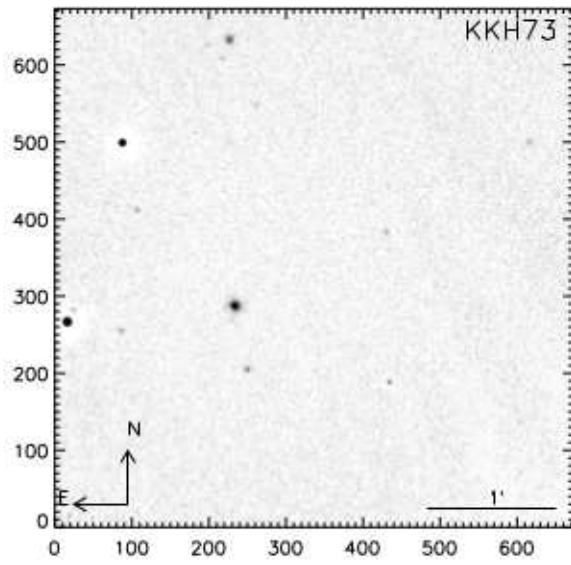
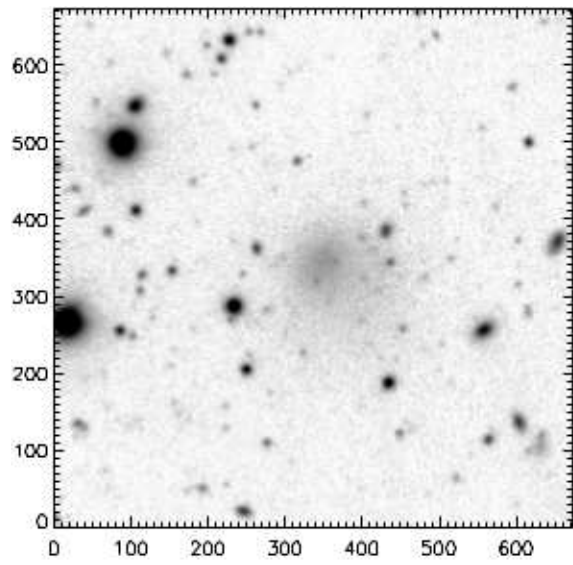


FIG. 1: Continued.

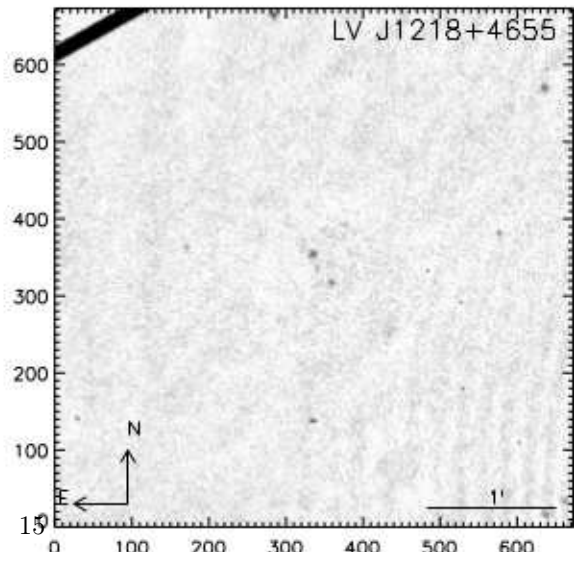
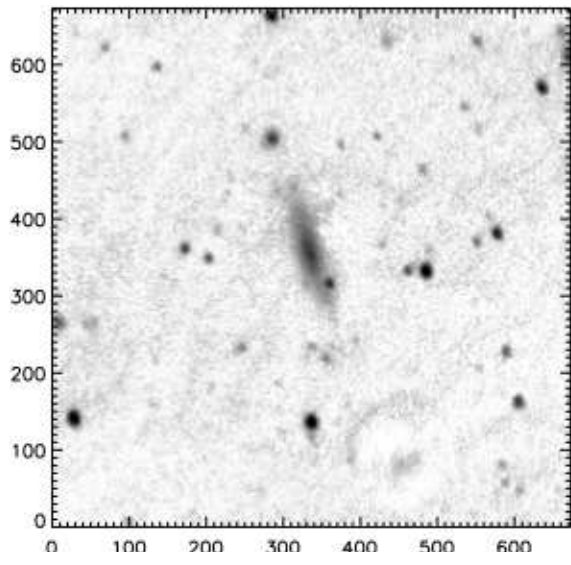
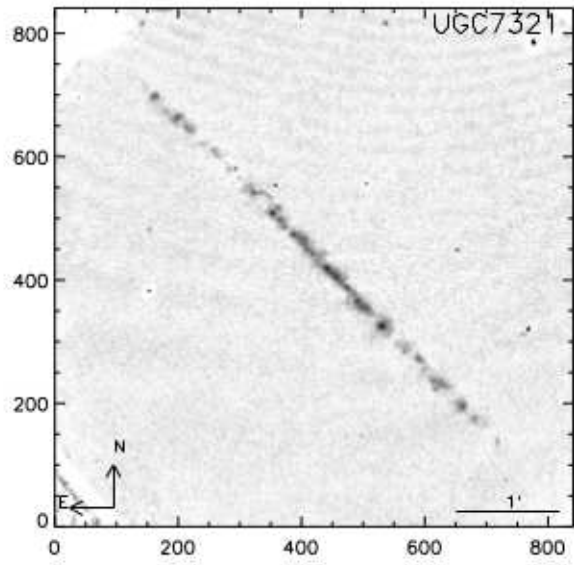
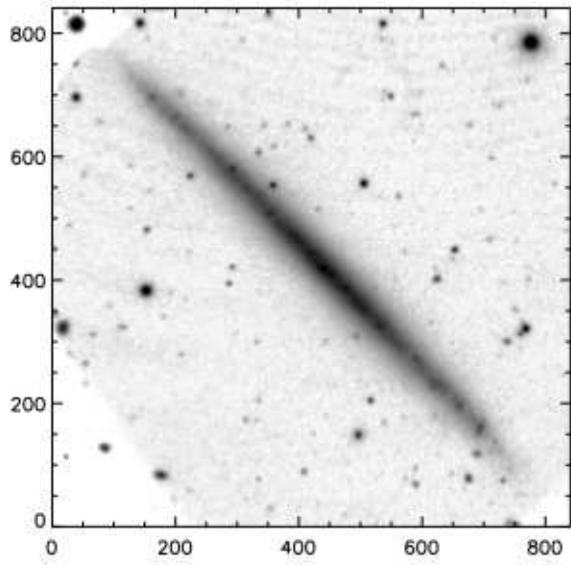
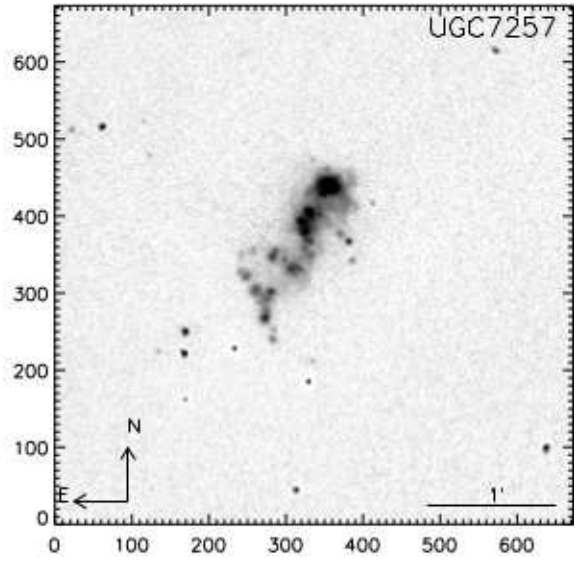
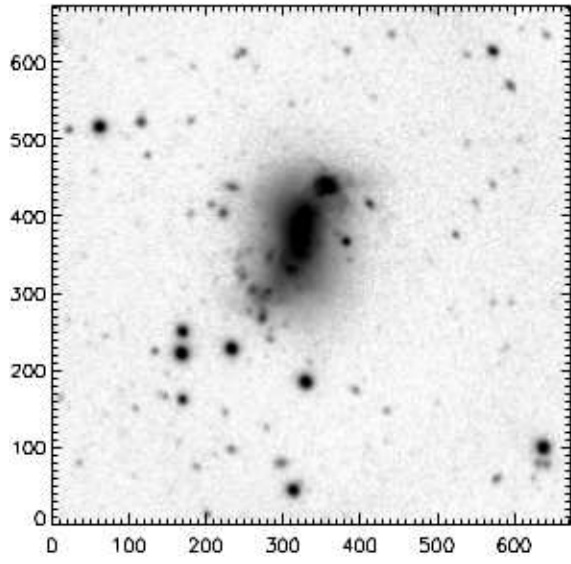


FIG. 1: Continued.

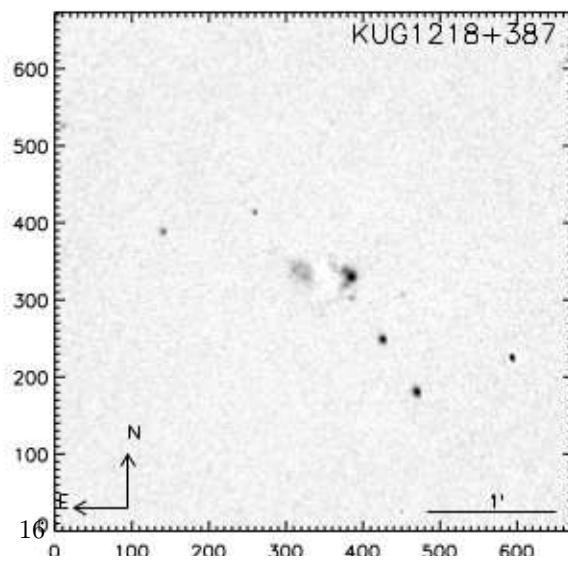
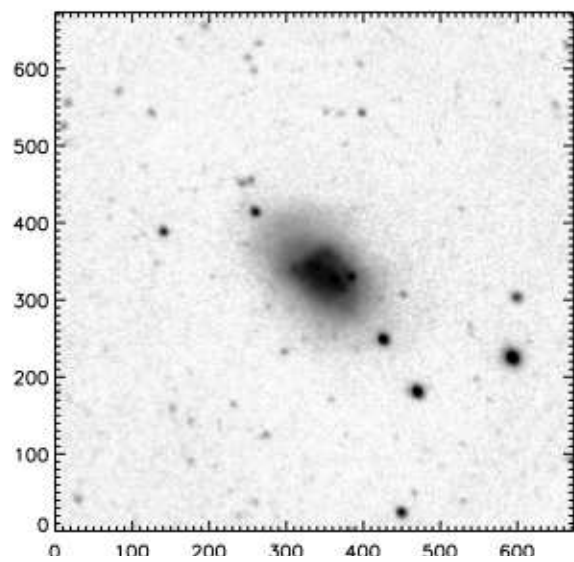
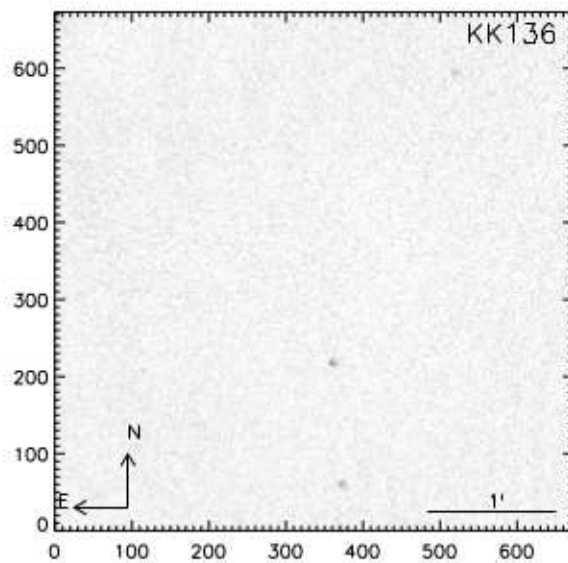
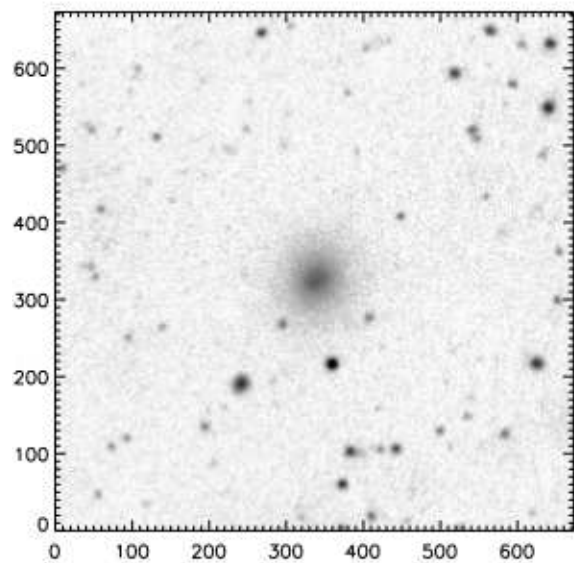
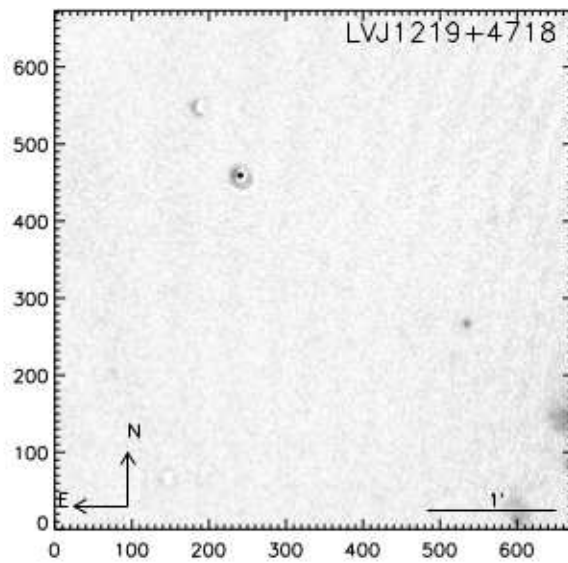
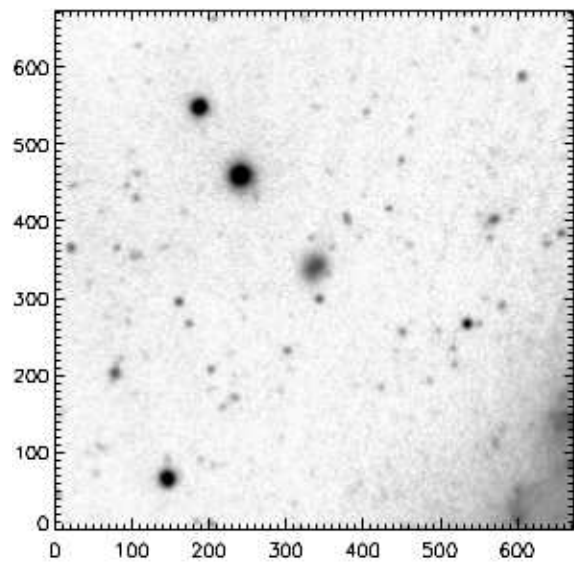


FIG. 1: Continued.

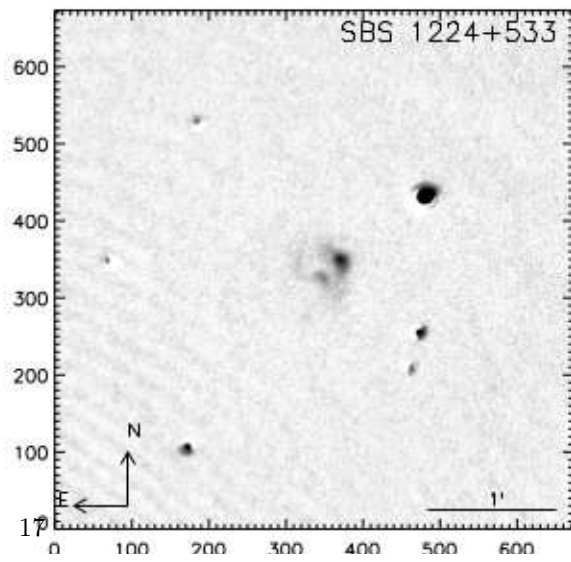
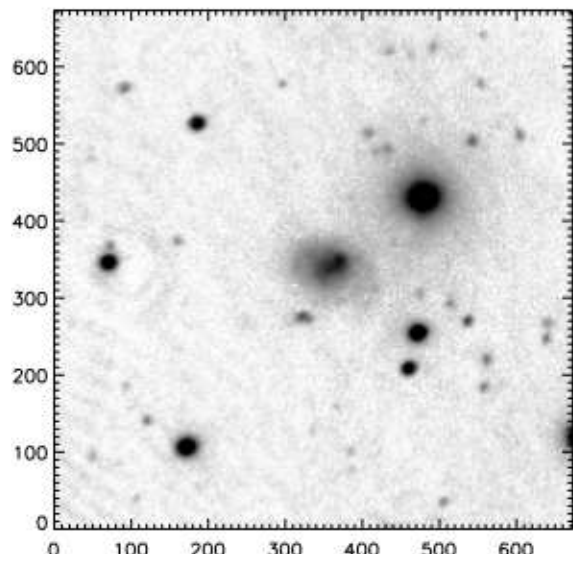
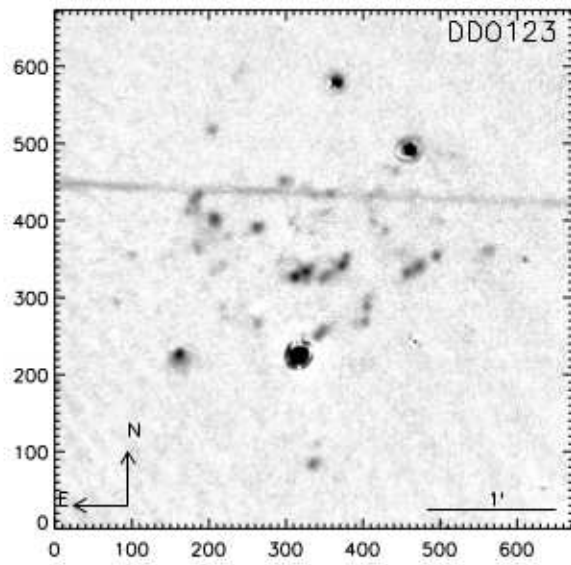
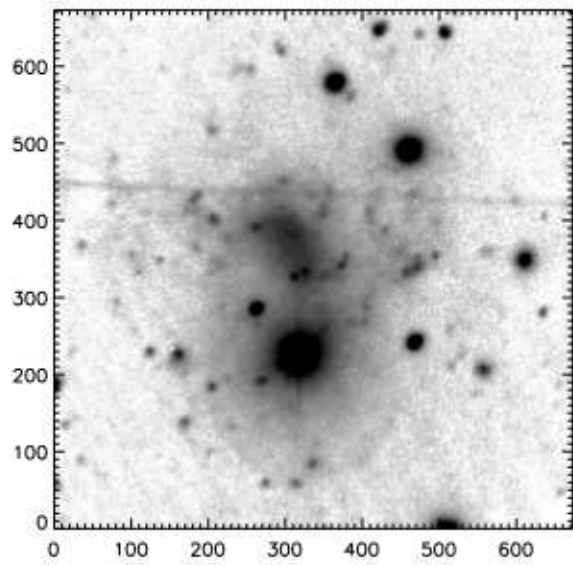
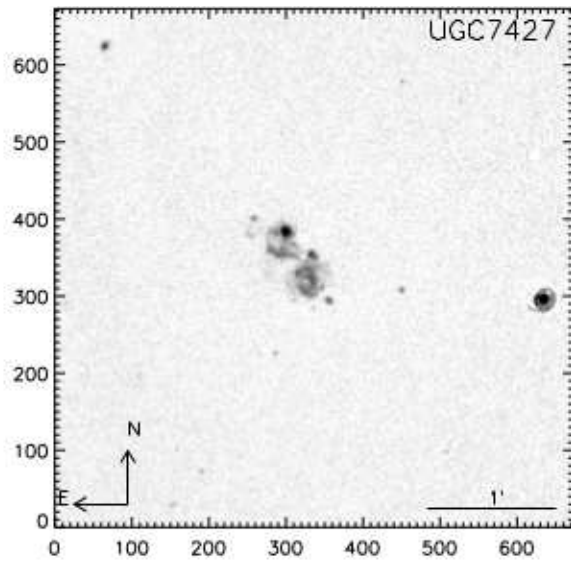
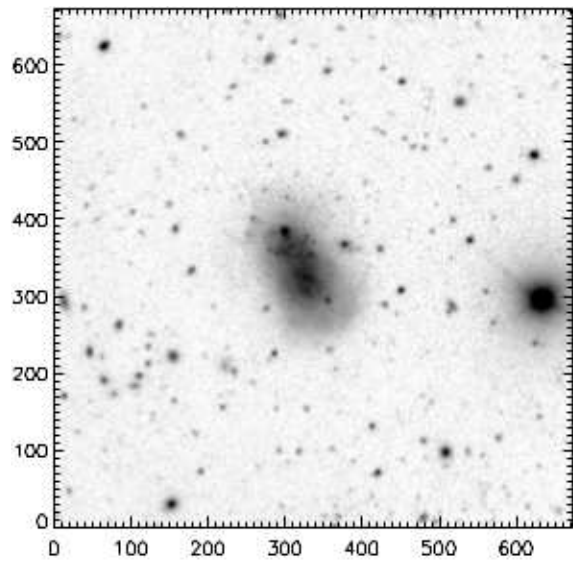


FIG. 1: Continued.

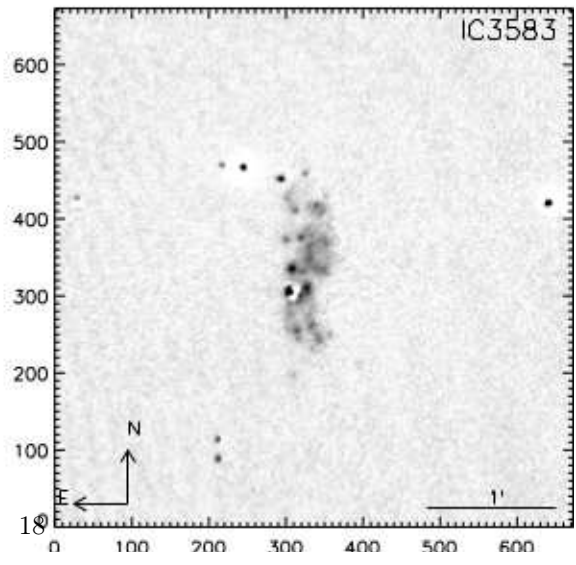
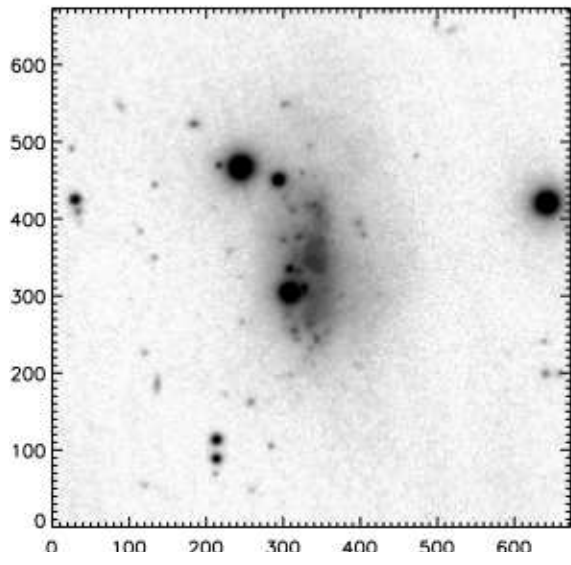
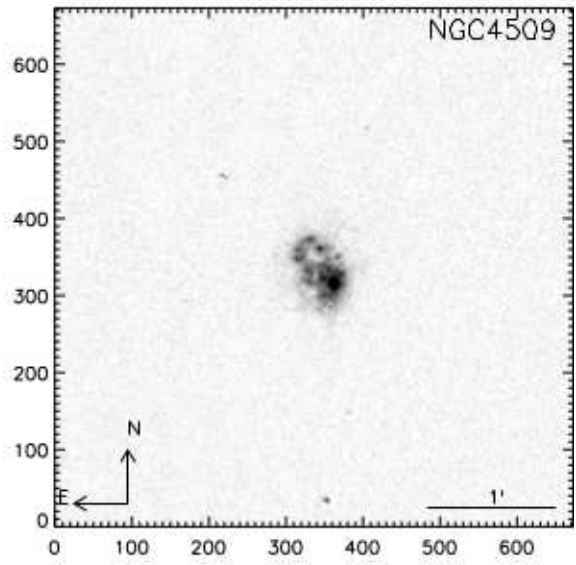
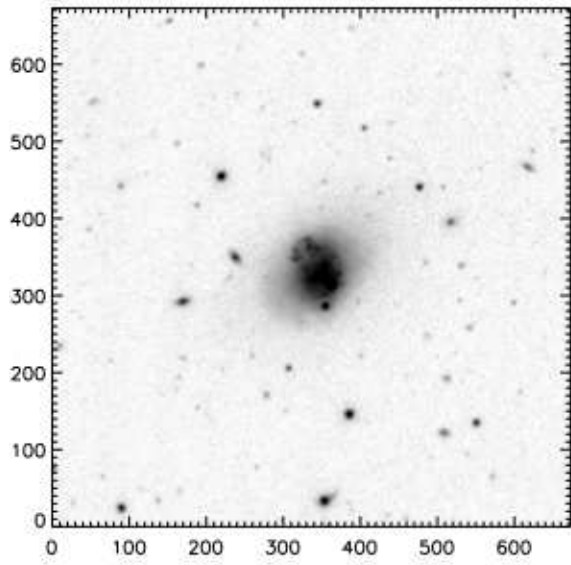
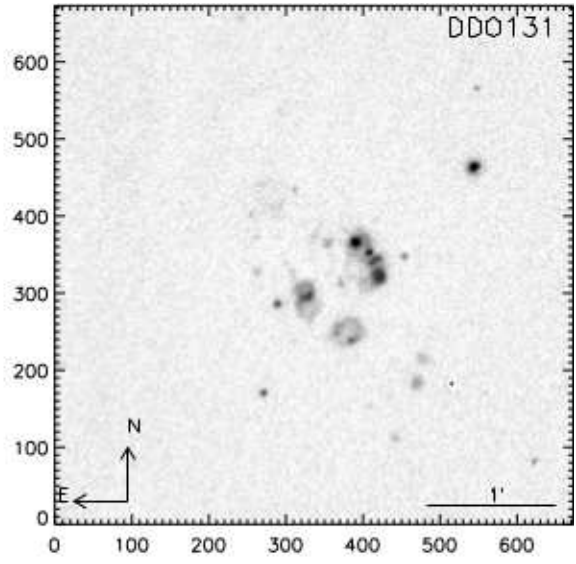
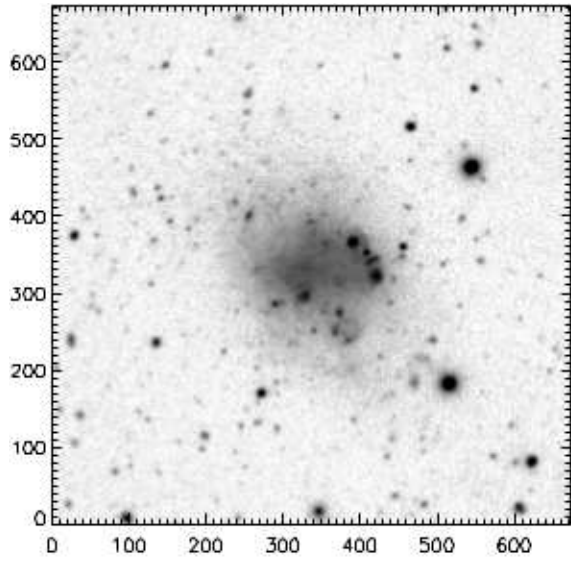


FIG. 1: Continued.

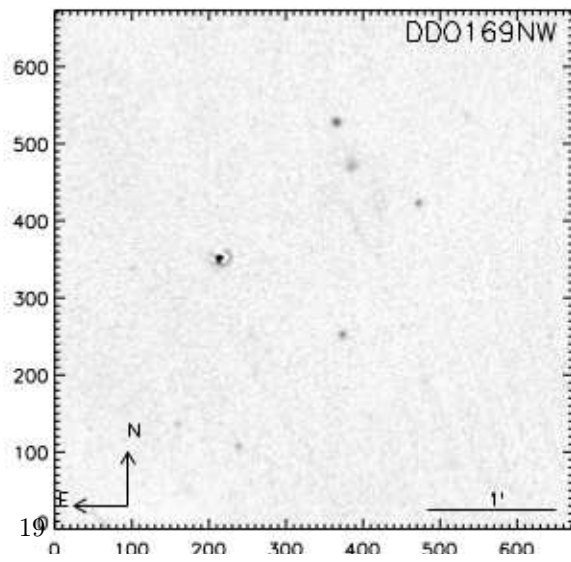
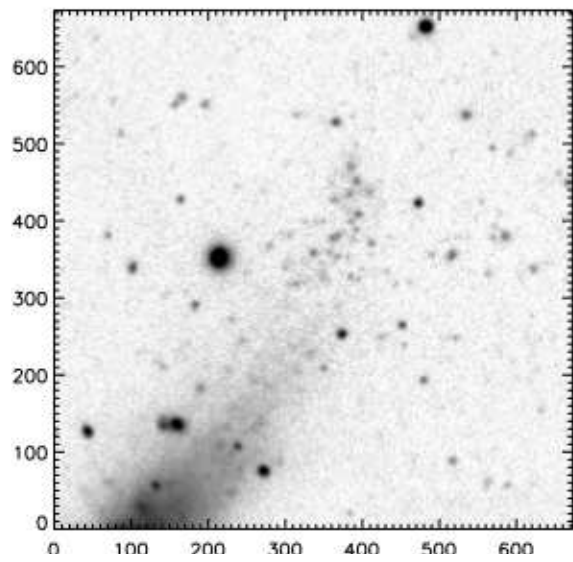
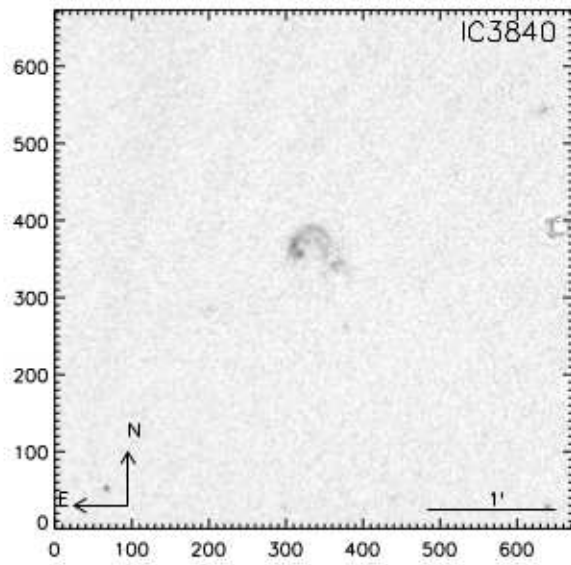
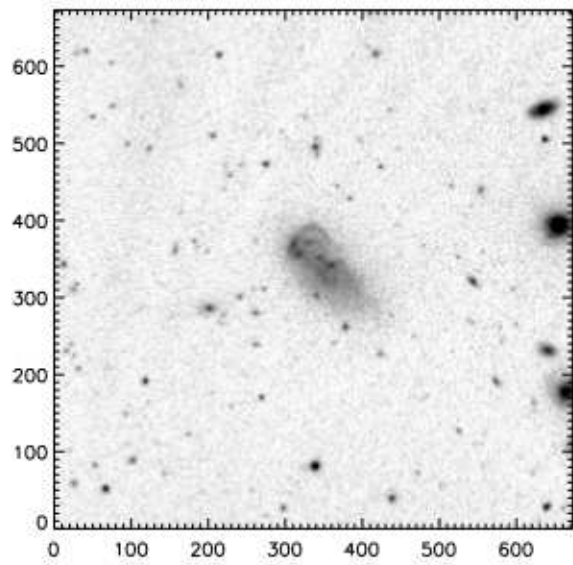
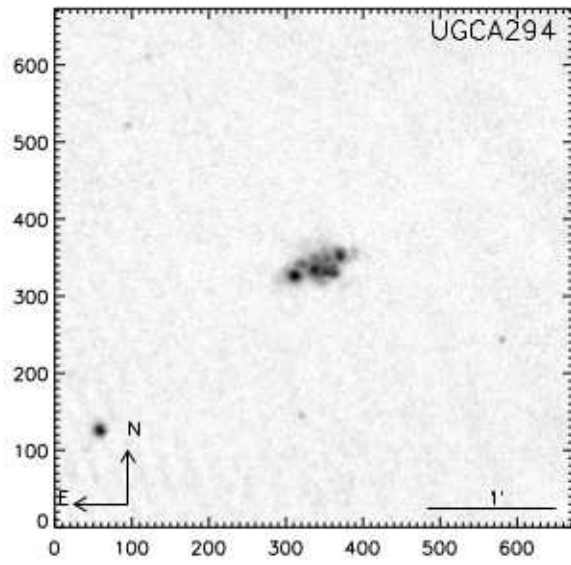
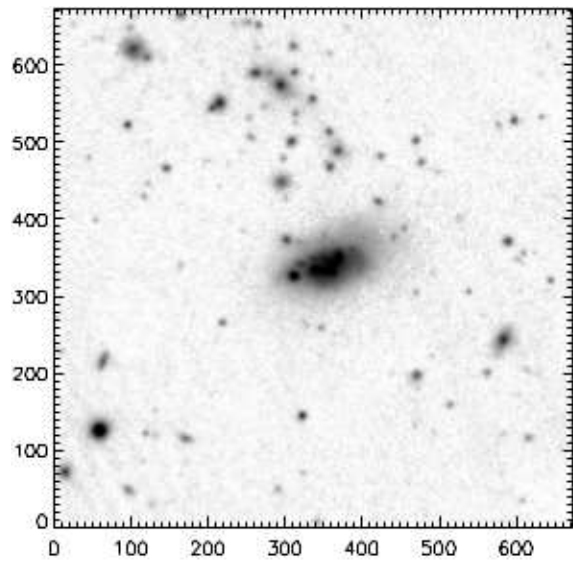


FIG. 1: Continued.

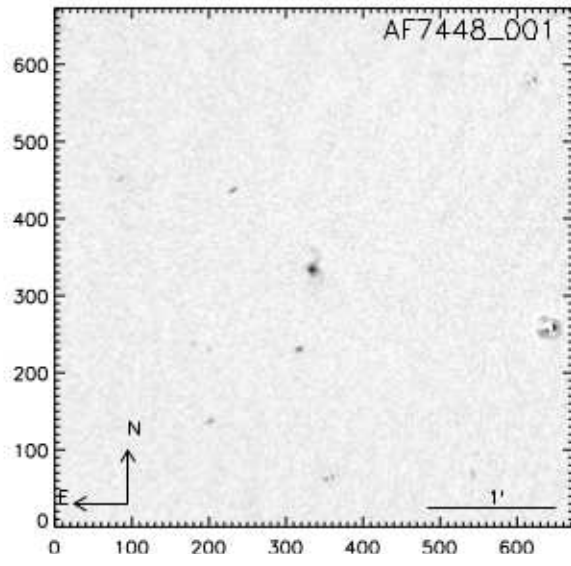
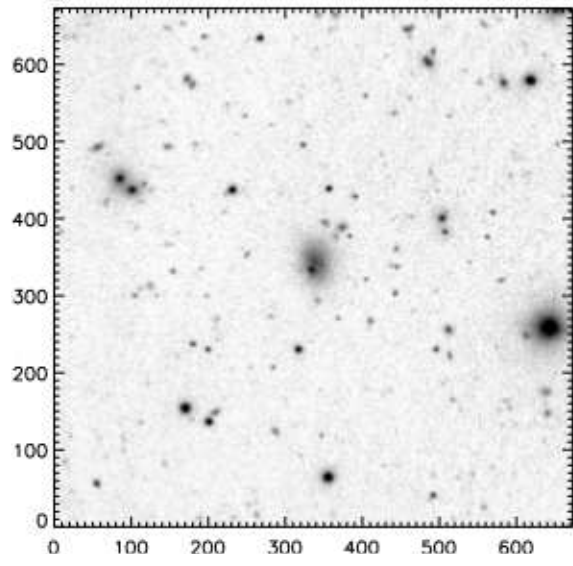
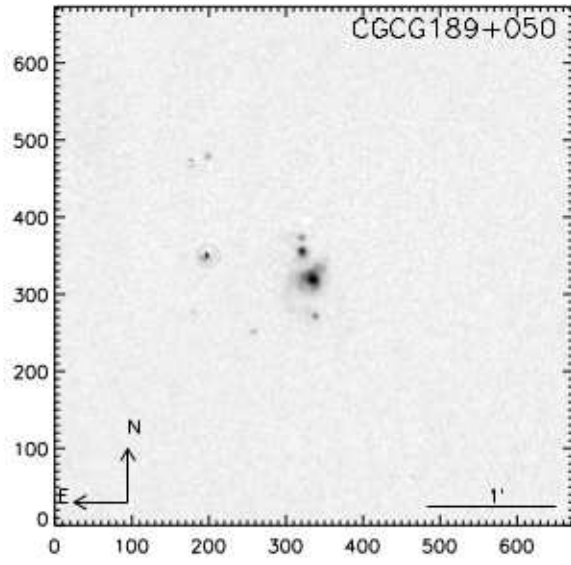
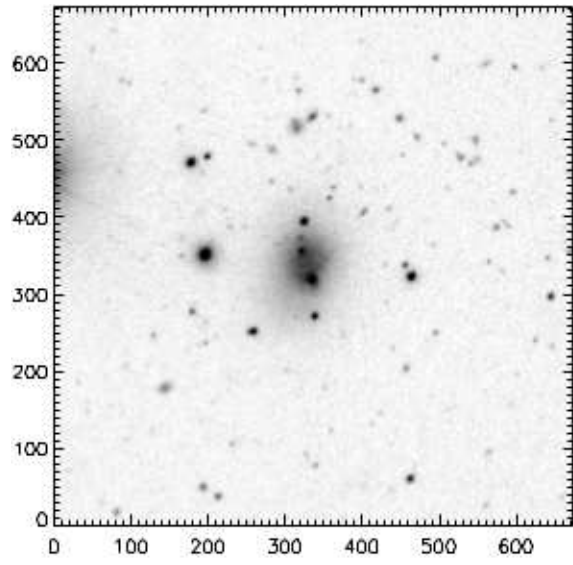


Рис. 1: Conclusion.